PLASTIC ANALYSIS OF INTERNALLY PRESSURIZED ALUMINUM PIPES STRENGTHENED WITH A COMPOSITE REPAIR

Alfredo R. de Faria, arfaria@ita.br
Instituto Tecnológico de Aeronáutica, Dept. of Mech. Eng., CTA-ITA-IEM, São José dos Campos, SP 12228–900, Brazil

André de Jesus, andre.dejesus@goodrich.com
Goodrich, 850 Lagoon Drive, Chula Vista, CA 91910, USA

Abstract. *This work assesses the plastic behavior of a pressurized aluminum pipe sealed at both ends with and without composite repair patches attached. The plastic behavior of the aluminum material is incorporated into the numerical analyses performed and the von Mises yield criterion with associated plasticity is adopted. The objective is to verify what the yield strength of the overall pipe is and what happens after yielding, depending on the configuration selected for the laminate patch and the severity of the damage in the metallic pipe. A finite element (FE) code is developed based on: (i) the bi-quadratic Lagrange element with 9 nodes, (ii) the Mindlin theory with out-of-plane shear strains, and (iii) orthotropic materials. The strain× displacement relations are assumed linear including the inherent shell curvature effect although the constitutive equation is nonlinear, accounting for plastic effects. The FE code results are compared against those obtained by the commercial package MSC.Nastran.*

Keywords*: plasticity, composite materials, finite elements, composite repair*

1. INTRODUCTION

As of the beginning of the eighties there is growing interest in the use of composite materials reinforced with fibers in the aeronautical and space businesses (Almeida, 1982; Levy Neto, 1983). Thereafter, is applicability has been widespread to the automotive, naval, chemical, oil and civil engineering applications. Examples of application include: structural aerospace components, shafts, pipes and pressure vessels, wet (marine) structures, trusses, masts, panels, sandwich beams, etc. Reinforced composites are increasingly important and its applicability to pipeline repair has been growing steadily (Levy Neto et al., 2000; Levy Neto et al., 2005). Brazilian experiences involving composites can are: (i) stabilizers of the SONDA IV rocket (Almeida, 1982), (ii) leading edges of the Embraer 120 aircraft (Levy Neto, 1983), (iii) motor case of the fourth stage of the VLS rocket (Palmério, Levy Neto, 1994; Levy Neto, Gonçalves, 2001). In the international scene, Boeing has recently launched an ambitious project of building a commercial jet mostly based on composite design: the 787 dreamliner.

Despite its advantages, the design of composite structures is complicated by the wide variety of matrix and fiber reinforcement materials available, the potential of stress concentrations, thermal residual stresses from the manufacturing process, the choice of ply thicknesses and number of plies, the necessity of considering riveted and bonded joints in large structures, and the spatial variation of ply orientation. Other design variables related to the structure topology and geometry are also often considered.

The objective of this paper is to present the calculations and simulations describing the elastic and plastic regimes a pressurized aluminum pipe sealed at both ends, with and without composite repair patches attached. The simulations conducted are based on a finite element code specially developed for this work based on the Mindlin theory (de Faria, 2000) where transverse shear effects are incorporated and a bi-quadratic Lagrange element with nine nodes (Hughes, 1987). The original pipe configuration assumed is that of a purely metallic cylinder worn out over a well defined region. A composite repair patch is then added on top of this weaker region and a new simulation is conducted to observe the stress re-distribution. The inherently nonlinear plastic analysis performed assumes the von Mises yield criterion with associated plasticity (Kachanov, 2004; Owen, 1980). The main objective of this nonlinear analysis is to gain insight into the plastic response of the repaired structure and to estimate the overall repaired pipe strength. The stress × strain relations are assumed linear and take into account the cylindrical shell curvature, although the constitutive equation is nonlinear, reflecting plastic effects. The FE code results are compared against those obtained by the commercial package MSC.Nastran.

2. IMPLEMENTATION OF THE LINEAR FINITE ELEMENT CODE

A finite element code for circular cylindrical orthotropic shells has been developed to conduct the necessary numerical simulations. This code assumes a linear elastic regime of the material but is the basis for the nonlinear plastic code to be introduced subsequently. The strain × displacement relations for circular cylindrical shells are:

$$\varepsilon_{xx}=\frac{\partial \bar{u}}{\partial x},\quad \varepsilon_{\theta\theta}=\frac{1}{R}\frac{\partial \bar{v}}{\partial \theta}+\frac{\bar{w}}{R},\quad \gamma_{x\theta}=\frac{1}{R}\frac{\partial \bar{u}}{\partial \theta}+\frac{\partial \bar{v}}{\partial x},\quad \gamma_{xz}=\frac{\partial \bar{u}}{\partial z}+\frac{\partial \bar{w}}{\partial x},\quad \gamma_{\theta z}=\frac{\partial \bar{v}}{\partial z}+\frac{1}{R}\frac{\partial \bar{w}}{\partial \theta}, \tag{1}$$

where x is the coordinate measured along the x axis, θ is the circumferential coordinate, z the coordinate along the axis perpendicular to the cylinder surface and $\bar{u}$, $\bar{v}$, $\bar{w}$ are the displacements of an arbitrary point of the cylinder, described along x, θ and z, respectively. In general, $\bar{u}$, $\bar{v}$, $\bar{w}$ are functions of x, θ and z. Equation (1) may be re-written assuming the circumferential coordinate $y = R\theta$ such that

$$\varepsilon_{xx}=\frac{\partial\bar{u}}{\partial x},\quad \varepsilon_{yy}=\frac{\partial\bar{v}}{\partial y}+\frac{\bar{w}}{R},\quad \gamma_{xy}=\frac{\partial\bar{u}}{\partial y}+\frac{\partial\bar{v}}{\partial x},\quad \gamma_{xz}=\frac{\partial\bar{u}}{\partial z}+\frac{\partial\bar{w}}{\partial x},\quad \gamma_{yz}=\frac{\partial\bar{v}}{\partial z}+\frac{\partial\bar{w}}{\partial y}-\frac{\bar{v}}{R}. \tag{2}$$

The finite element implemented follows the Mindlin theory according to which:

$$\bar{u}(x,y,z)=u(x,y)+z\psi_x(x,y),\quad \bar{v}(x,y,z)=v(x,y)+z\psi_y(x,y),\quad \bar{w}(x,y,z)=w(x,y). \tag{3}$$

Defining vectors

$$\boldsymbol{\varepsilon}_0=\begin{Bmatrix} u_{,x} \\ v_{,y}+w/R \\ u_{,x}+v_{,y}\end{Bmatrix}\quad \boldsymbol{\kappa}_p=\begin{Bmatrix} \psi_{x,x} \\ \psi_{y,y} \\ \psi_{x,y}+\psi_{y,x}\end{Bmatrix}\quad \boldsymbol{\gamma}_0=\begin{Bmatrix} w_{,x}+\psi_x \\ w_{,y}+\psi_y-v/R\end{Bmatrix}\quad \boldsymbol{\kappa}_s=\begin{Bmatrix} 0 \\ -\psi_y/R\end{Bmatrix}, \tag{4}$$

the expression for the total potential energy is

$$\Pi=\frac{1}{2}\int_\Omega\begin{Bmatrix}\boldsymbol{\varepsilon}_0\\ \boldsymbol{\kappa}_p\end{Bmatrix}^T\begin{bmatrix}\mathbf{A} & \mathbf{B}\\ \mathbf{B} & \mathbf{D}\end{bmatrix}\begin{Bmatrix}\boldsymbol{\varepsilon}_0\\ \boldsymbol{\kappa}_p\end{Bmatrix}d\Omega+\frac{1}{2}\int_\Omega\begin{Bmatrix}\boldsymbol{\gamma}_0\\ \boldsymbol{\kappa}_s\end{Bmatrix}^T\begin{bmatrix}\mathbf{A}_s & \mathbf{B}_s\\ \mathbf{B}_s & \mathbf{D}_s\end{bmatrix}\begin{Bmatrix}\boldsymbol{\gamma}_0\\ \boldsymbol{\kappa}_s\end{Bmatrix}d\Omega-$$
$$\int_\Omega pw\,d\Omega-\int_0^{2\pi R}\bar{N}_{xx}u(L,y)dy-\int_0^{2\pi R}\bar{N}_{xy}v(L,y)dy+\int_0^{2\pi R}\bar{N}_{xx}u(-L,y)dy+\int_0^{2\pi R}\bar{N}_{xy}v(-L,y)dy \tag{5}$$

In Eq. (5) it is assumed that a uniform normal membrane force $\bar{N}_{xx}$ exists in the longitudinal direction and a uniform shear membrane force $\bar{N}_{xy}$ exists. Matrices **A**, **B**, **D**, $\mathbf{A}_s$, $\mathbf{B}_s$ and $\mathbf{D}_s$ are defined based on the constitutive equations of each lamina in the laminate, that is,

$$\begin{Bmatrix}\sigma_{xx}\\ \sigma_{yy}\\ \tau_{xy}\end{Bmatrix}=\bar{\mathbf{Q}}\begin{Bmatrix}\varepsilon_{xx}\\ \varepsilon_{yy}\\ \gamma_{xy}\end{Bmatrix}\qquad \begin{Bmatrix}\tau_{xz}\\ \tau_{yz}\end{Bmatrix}=\bar{\mathbf{Q}}_s\begin{Bmatrix}\gamma_{xz}\\ \gamma_{yz}\end{Bmatrix}, \tag{6}$$

and matrices **A**, **B**, **D**, $\mathbf{A}_s$, $\mathbf{B}_s$ and $\mathbf{D}_s$ are given by

$$\mathbf{A}=\int_0^t\bar{\mathbf{Q}}dz,\quad \mathbf{B}=\int_0^t\bar{\mathbf{Q}}dz,\quad \mathbf{D}=\int_0^t\bar{\mathbf{Q}}dz,\quad \mathbf{A}_s=\int_0^t\bar{\mathbf{Q}}_s dz,\quad \mathbf{B}_s=\int_0^t\bar{\mathbf{Q}}_s dz,\quad \mathbf{D}_s=\int_0^t\bar{\mathbf{Q}}_s dz. \tag{7}$$

It is observed in Eq. (7) that the integrals are evaluated from 0 to t, where t is the total laminate thickness. These definitions for **A**,..., $\mathbf{D}_s$ are not those traditionally found when the integration is from $-t/2$ to $+t/2$. The difference lies in the location of the reference surface. In Eq. (7) the reference surface is the innermost whereas traditionally the mid surface is assumed as the reference surface. Equation (5) is the basis for the discretization employed in finite element method. Figure 1 shows the bi-quadratic finite element implemented with 9 nodes. The applicable interpolation functions are

$$\begin{aligned}
&\phi_1(\xi,\eta)=\frac{1}{4}\xi(\xi-1)\eta(\eta-1) \quad \phi_2(\xi,\eta)=\frac{1}{2}(1-\xi^2)\eta(\eta-1) \quad \phi_3(\xi,\eta)=\frac{1}{4}\xi(\xi+1)\eta(\eta-1)\\
&\phi_4(\xi,\eta)=\frac{1}{2}\xi(\xi-1)(1-\eta^2) \quad \phi_5(\xi,\eta)=(1-\xi^2)(1-\eta^2) \quad \phi_6(\xi,\eta)=\frac{1}{2}\xi(\xi+1)(1-\eta^2)\\
&\phi_7(\xi,\eta)=\frac{1}{4}\xi(\xi-1)\eta(\eta+1) \quad \phi_8(\xi,\eta)=\frac{1}{2}(1-\xi^2)\eta(\eta+1) \quad \phi_9(\xi,\eta)=\frac{1}{4}\xi(\xi+1)\eta(\eta+1)
\end{aligned}, \tag{8}$$

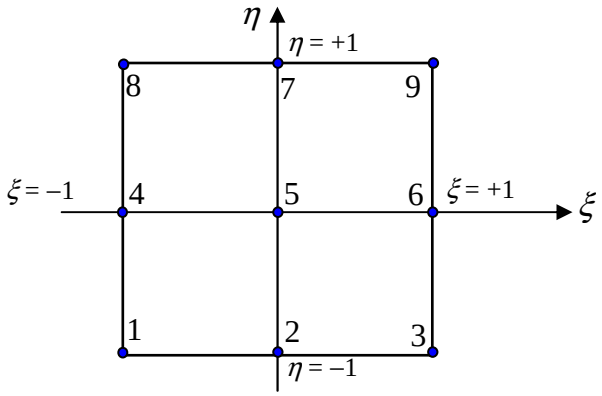

Figure 1. Bi-quadratic finite element

From the interpolation functions ϕ_i presented in Eq. (8) a number of useful vectors can be defined:

$$\begin{aligned}
&\mathbf{q}_u=\{u_1\ u_2\ u_3\ u_4\ u_5\ u_6\ u_7\ u_8\ u_9\}^T\\
&\mathbf{q}_v=\{v_1\ v_2\ v_3\ v_4\ v_5\ v_6\ v_7\ v_8\ v_9\}^T\\
&\mathbf{q}_w=\{w_1\ w_2\ w_3\ w_4\ w_5\ w_6\ w_7\ w_8\ w_9\}^T\\
&\mathbf{q}_{\psi_x}=\{\psi_{x1}\ \psi_{x2}\ \psi_{x3}\ \psi_{x4}\ \psi_{x5}\ \psi_{x6}\ \psi_{x7}\ \psi_{x8}\ \psi_{x9}\}^T\\
&\mathbf{q}_{\psi_y}=\{\psi_{y1}\ \psi_{y2}\ \psi_{y3}\ \psi_{y4}\ \psi_{y5}\ \psi_{y6}\ \psi_{y7}\ \psi_{y8}\ \psi_{y9}\}^T\\
&\boldsymbol{\varphi}=[\phi_1\ \phi_2\ \phi_3\ \phi_4\ \phi_5\ \phi_6\ \phi_7\ \phi_8\ \phi_9]\\
&\mathbf{q}=\{\mathbf{q}_u^T\ \mathbf{q}_v^T\ \mathbf{q}_w^T\ \mathbf{q}_{\psi_x}^T\ \mathbf{q}_{\psi_y}^T\}^T
\end{aligned}, \tag{9}$$

where u_i, v_i, w_i, ψ_{xi} e ψ_{yi} are the nodal degrees of freedom of node i. The problem discretization follows from Eqs. (8) and (9). Within any element the displacements and rotations are interpolated:

$$u=\boldsymbol{\varphi}\mathbf{q}_u \qquad v=\boldsymbol{\varphi}\mathbf{q}_v \qquad w=\boldsymbol{\varphi}\mathbf{q}_w \qquad \psi_x=\boldsymbol{\varphi}\mathbf{q}_{\psi_x} \qquad \psi_y=\boldsymbol{\varphi}\mathbf{q}_{\psi_y}. \tag{10}$$

The strain relations shown in Eq. (4) can also be discretized with Eq. (10) yielding

$$\begin{Bmatrix}\boldsymbol{\varepsilon}_0\\ \boldsymbol{\kappa}_p\end{Bmatrix}=\begin{bmatrix}\boldsymbol{\varphi}_{,x} & \mathbf{0} & \mathbf{0} & \mathbf{0} & \mathbf{0}\\ \mathbf{0} & \boldsymbol{\varphi}_{,y} & \boldsymbol{\varphi}/R & \mathbf{0} & \mathbf{0}\\ \boldsymbol{\varphi}_{,y} & \boldsymbol{\varphi}_{,x} & \mathbf{0} & \mathbf{0} & \mathbf{0}\\ \mathbf{0} & \mathbf{0} & \mathbf{0} & \boldsymbol{\varphi}_{,x} & \mathbf{0}\\ \mathbf{0} & \mathbf{0} & \mathbf{0} & \mathbf{0} & \boldsymbol{\varphi}_{,y}\\ \mathbf{0} & \mathbf{0} & \mathbf{0} & \boldsymbol{\varphi}_{,y} & \boldsymbol{\varphi}_{,x}\end{bmatrix}\mathbf{q}=\boldsymbol{\Phi}\mathbf{q} \quad \begin{Bmatrix}\boldsymbol{\gamma}_0\\ \boldsymbol{\kappa}_s\end{Bmatrix}=\begin{bmatrix}\mathbf{0} & \mathbf{0} & \boldsymbol{\varphi}_{,x} & \boldsymbol{\varphi} & \mathbf{0}\\ \mathbf{0} & -\boldsymbol{\varphi}/R & \boldsymbol{\varphi}_{,y} & \mathbf{0} & \boldsymbol{\varphi}\\ \mathbf{0} & \mathbf{0} & \mathbf{0} & \mathbf{0} & \mathbf{0}\\ \mathbf{0} & \mathbf{0} & \mathbf{0} & \mathbf{0} & -\boldsymbol{\varphi}/R\end{bmatrix}\mathbf{q}=\boldsymbol{\Phi}_s\mathbf{q}. \tag{11}$$

The derivatives of the interpolation functions ϕ_i in Eq. (11) are taken with respect to the global coordinates x, y. However, the interpolation functions are defined in terms of element local coordinates ξ, η. In order to make the change of variables the usual jacobian matrix must be computed. Isoparametric mapping is adopted, i.e., the same interpolation functions used for displacements are used for coordinates.

Substitution of Eq. (11) in Eq. (5) leads

$$\Pi=\frac{1}{2}\int_{\Omega}\mathbf{q}^T\boldsymbol{\Phi}^T\begin{bmatrix}\mathbf{A} & \mathbf{B}\\ \mathbf{B} & \mathbf{D}\end{bmatrix}\boldsymbol{\Phi}\mathbf{q}\,d\Omega+\frac{1}{2}\int_{\Omega}\mathbf{q}^T\boldsymbol{\Phi}_s^T\begin{bmatrix}\mathbf{A}_s & \mathbf{B}_s\\ \mathbf{B}_s & \mathbf{D}_s\end{bmatrix}\boldsymbol{\Phi}_s\mathbf{q}\,d\Omega-$$
$$\int_{\Omega}p\boldsymbol{\varphi}\mathbf{q}_w\,d\Omega-\int_0^{2\pi R}\bar{N}_{xx}(\boldsymbol{\varphi}\mathbf{q}_l)_{x=L}\,dy-\int_0^{2\pi R}\bar{N}_{xy}(\boldsymbol{\varphi}\mathbf{q}_l)_{x=L}\,dy+\int_0^{2\pi R}\bar{N}_{xx}(\boldsymbol{\varphi}\mathbf{q}_l)_{x=-L}\,dy+\int_0^{2\pi R}\bar{N}_{xy}(\boldsymbol{\varphi}\mathbf{q}_l)_{x=-L}\,dy \quad . \tag{12}$$

From Eq. (12) the element stiffness matrix $\mathbf{K}_e$ and the element load vector $\mathbf{f}_e$ are:

$$\mathbf{K}_e=\int_{\Omega_e}\boldsymbol{\Phi}^T\begin{bmatrix}\mathbf{A} & \mathbf{B}\\ \mathbf{B} & \mathbf{D}\end{bmatrix}\boldsymbol{\Phi}\,d\Omega+\int_{\Omega_e}\boldsymbol{\Phi}_s^T\begin{bmatrix}\mathbf{A}_s & \mathbf{B}_s\\ \mathbf{B}_s & \mathbf{D}_s\end{bmatrix}\boldsymbol{\Phi}_s\,d\Omega$$
$$\mathbf{f}_e=\int_{\Omega_e}p\begin{Bmatrix}\mathbf{0}^T\\ \mathbf{0}^T\\ \boldsymbol{\varphi}^T\\ \mathbf{0}^T\\ \mathbf{0}^T\end{Bmatrix}d\Omega-\int_0^{2\pi R}\left(\bar{N}_{xx}\begin{Bmatrix}\boldsymbol{\varphi}^T\\ \mathbf{0}^T\\ \mathbf{0}^T\\ \mathbf{0}^T\\ \mathbf{0}^T\end{Bmatrix}_{x=L}+\bar{N}_{xy}\begin{Bmatrix}\mathbf{0}^T\\ \boldsymbol{\varphi}^T\\ \mathbf{0}^T\\ \mathbf{0}^T\\ \mathbf{0}^T\end{Bmatrix}_{x=L}-\bar{N}_{xx}\begin{Bmatrix}\boldsymbol{\varphi}^T\\ \mathbf{0}^T\\ \mathbf{0}^T\\ \mathbf{0}^T\\ \mathbf{0}^T\end{Bmatrix}_{x=-L}-\bar{N}_{xy}\begin{Bmatrix}\mathbf{0}^T\\ \boldsymbol{\varphi}^T\\ \mathbf{0}^T\\ \mathbf{0}^T\\ \mathbf{0}^T\end{Bmatrix}_{x=-L}\right)dy \quad . \tag{13}$$

Equation (13b) must be carefully interpreted. Only elements that possess one edge coincident on the cylinder edges ($x = \pm L$) will have their load vectors affected by the second integral from 0 to $2\pi R$.

The integrations required to computing the element stiffness matrices and load vectors are done numerically through Gauss quadrature. For the bi-quadratic element it is recommended the use of the 3-point quadrature per direction, with a total of 9 points in two dimensions. However, the formulation based on the Mindlin theory leads a well-known numerical flaw: shear locking. This problem can be overcome by reduced selective integration. Hence, the first integral in Eq. (13a) and the load vector are obtained with 9 points whereas the second integral is computed with only 4 points (2 per direction).

2.1. Linear elastic analysis of a damaged pipe

The constitutive laws presented in Eq. (6) are applicable to composites as well as isotropic materials, with changes in the $\overline{\mathbf{Q}}$ and $\overline{\mathbf{Q}}_s$ matrices. Therefore, initially only metallic cylinders were simulated. The simulation of a damaged metallic cylinder is done assuming a cylinder with two distinct regions: one (intact) with 2 mm thickness and one (damaged) with 1 mm thickness, as shown in Fig. 2. The cylinder has total length L = 1 m, radius R = 7.5 cm, Young modulus 210 GPa and Poisson coefficient 0.3. The length of the damaged region is l = 125 mm.

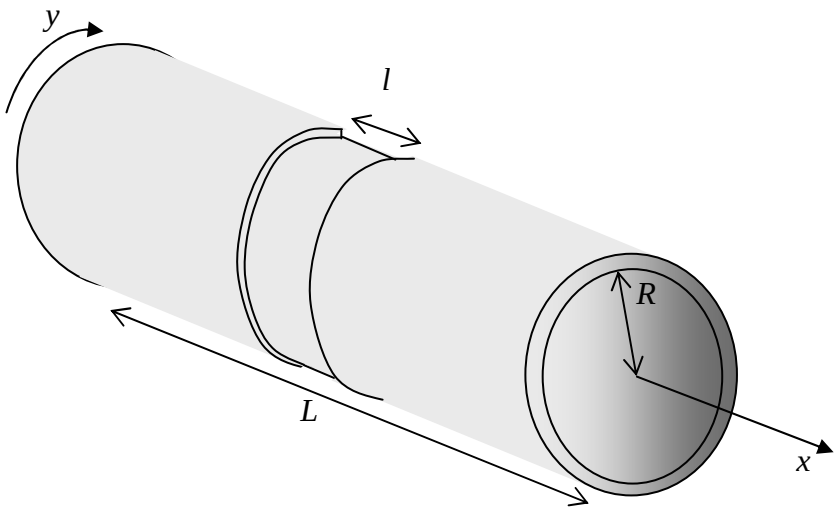

Figure 2. Damaged metallic cylinder

The applicable boundary conditions correspond to infinitely rigid caps, i.e., zero displacements v, w, ψ_x e ψ_y. This condition allows for displacement in the longitudinal direction only. The applied load is divided in two parts: pressure in the cylinder radial direction and longitudinal membrane forces of magnitude $\pi p R^2$ on the cylinder edges, where p = 1 atm. Under these conditions the result obtained is illustrated in Fig. 3 where it can be seen a detail confirming the presence of high gradients in the interface between intact and damaged zones. The solution seen in Fig. 3 is obviously axi-symmetric.

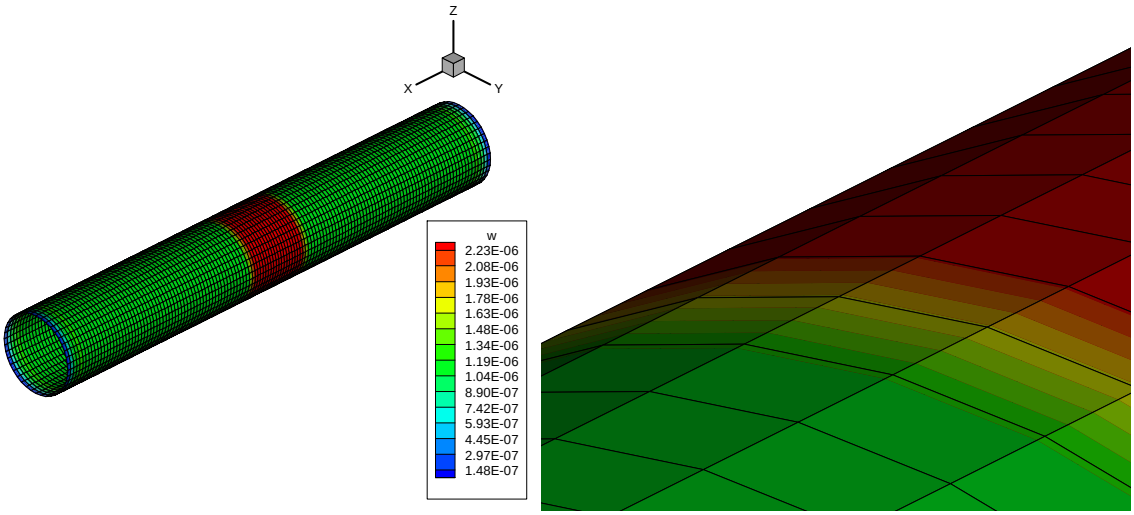

Figure 3. Damaged metallic cylinder under internal pressure

Figure 4 shows the variation of w with x and facilitates the observation of the strong gradients as seen in Fig. 3. The edge effects near the cylinder extremities as well as the potential deleterious effect of the damaged region can be fully appreciated.

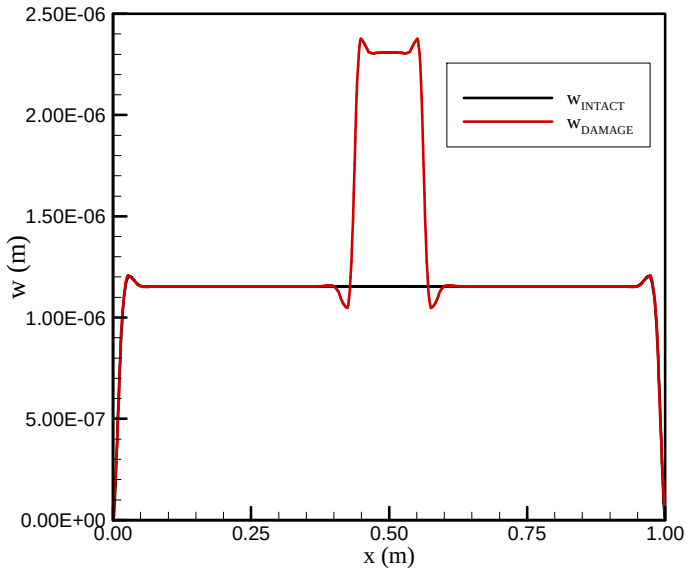

Figure 4. Damaged metallic cylinder: edge effects

3. NUMERICAL METHODS IN PLASTICITY

Through displacement based formulations several solid mechanics problems may be written as:

$$\boldsymbol{\psi}(\mathbf{q}) = \int \boldsymbol{\Phi}^T \boldsymbol{\sigma} d\Omega - \mathbf{f} = \mathbf{P}(\mathbf{q}) - \mathbf{f} = \mathbf{0}, \tag{14}$$

where matrix $\mathbf{\Phi}$ is presented in Eq. (11). Displacements and deformations may be approximated by

$$\mathbf{u}=\mathbf{N}\mathbf{q} \qquad \boldsymbol{\varepsilon}=\mathbf{\Phi}\mathbf{q}. \tag{15}$$

In general, $\boldsymbol{\sigma}$ depends on $\boldsymbol{\varepsilon}$ in a nonlinear fashion and, moreover, depends on the loading path followed. The tangential stiffness matrix is defined as

$$\mathbf{K}_T=\frac{\partial\boldsymbol{\psi}}{\partial\mathbf{q}}=\int\mathbf{\Phi}^T\frac{\partial\boldsymbol{\sigma}}{\partial\boldsymbol{\varepsilon}}\frac{\partial\boldsymbol{\varepsilon}}{\partial\mathbf{q}}d\Omega=\int\mathbf{\Phi}^T\mathbf{D}_T\mathbf{\Phi}d\Omega, \tag{16}$$

where

$$\mathbf{D}_T=\frac{\partial\boldsymbol{\sigma}}{\partial\boldsymbol{\varepsilon}}. \tag{17}$$

The form assumed by matrix $\mathbf{K}_T$ in Eq. (16) is particularly convenient since it is the exactly the form obtained in the theory of elasticity. In the case of nonlinear elasticity (hyperelasticity), the stress × strain relation is unique and path independent. On the other hand, plastic effects depend on the loading path and, particularly, depend on loading or unloading. In order to employ the laws of plasticity it is necessary to know when the material enters plastic regime. This point is known as yield point and it is located on a yield surface given by:

$$F(\boldsymbol{\sigma},\kappa)=0, \tag{18}$$

where κ is the hardening parameter. This yielding condition can be visualized as a surface in the stress space whose position and orientation depend on parameter κ. Von Mises was the first one to suggest that the basic behavior of plastic strain increments relates to the yield surface. Nowadays, the normality principle is widespread: if $d\boldsymbol{\varepsilon}^p$ is the plastic strain increment then

$$d\boldsymbol{\varepsilon}^p=d\lambda\frac{\partial F}{\partial\boldsymbol{\sigma}}, \tag{19}$$

where $d\lambda$ is a proportionality constant. The principle is known as normality principle since it requires $d\boldsymbol{\varepsilon}^p$ to be perpendicular to surface F. Restrictions to this model may be removed if a plastic potential $Q = Q(\boldsymbol{\sigma},\kappa)$ is defined such that Eq. (19) is valid just replacing F by Q. The case when $Q = F$ is known as associated plasticity.

During an infinitesimal stress increment the resulting strains can be split into elastic and plastic components. This is known as additive decomposition as opposed to multiplicative decomposition required in large strain problems. Thus,

$$d\boldsymbol{\varepsilon}=d\boldsymbol{\varepsilon}^e+d\boldsymbol{\varepsilon}^p=\mathbf{D}^{-1}d\boldsymbol{\sigma}+\frac{\partial Q}{\partial\boldsymbol{\sigma}}d\lambda. \tag{20}$$

The plastic strain increment $d\boldsymbol{\varepsilon}^p$ is present only if the elastic stress increment $d\boldsymbol{\sigma}^e = \mathbf{D}d\boldsymbol{\varepsilon}$ tends to push the stresses outside the yield surface, i.e., if it is in the direction of plastic loading. If, on the other hand, $d\boldsymbol{\sigma}^e$ is such that unloading occurs, then there is no plastic strain. This test is therefore essential to differ between loading and unloading, and emphasizes the importance of the loading path followed. When plastic loading occurs, the stresses are on the yield surface given by Eq. (18). Differentiating Eq. (18),

$$dF=\frac{\partial F}{\partial\sigma_1}d\sigma_1+\frac{\partial F}{\partial\sigma_2}d\sigma_2+...+\frac{\partial F}{\partial\kappa}d\kappa=\left(\frac{\partial F}{\partial\boldsymbol{\sigma}}\right)^T d\boldsymbol{\sigma}+\frac{\partial F}{\partial\kappa}d\kappa=0. \tag{21}$$

Defining

$$A=-\frac{\partial F}{\partial\kappa}\frac{d\kappa}{d\lambda}, \tag{22}$$

Eqs. (20) and (21) can be written as

$$\begin{Bmatrix} d\boldsymbol{\varepsilon} \\ 0 \end{Bmatrix} = \begin{bmatrix} \mathbf{D}^{-1} & \dfrac{\partial Q}{\partial \boldsymbol{\sigma}} \\ \left(\dfrac{\partial F}{\partial \boldsymbol{\sigma}}\right)^T & -A \end{bmatrix} \begin{Bmatrix} d\boldsymbol{\sigma} \\ d\lambda \end{Bmatrix}. \tag{23}$$

The constant $d\lambda$ may now be eliminated from Eq. (23). Multiplying the first line of Eq. (23) by $(\partial F/\partial \boldsymbol{\sigma})^T\mathbf{D}$ and substituting the result into the second line of Eq. (23) gives

$$\left(\frac{\partial F}{\partial \boldsymbol{\sigma}}\right)^T \mathbf{D} d\boldsymbol{\varepsilon} - \left[\left(\frac{\partial F}{\partial \boldsymbol{\sigma}}\right)^T \mathbf{D}\left(\frac{\partial Q}{\partial \boldsymbol{\sigma}}\right) + A\right] d\lambda = 0, \tag{24}$$

which plugged back into Eq. (23) yields

$$d\boldsymbol{\sigma} = \left\{\mathbf{D} - \mathbf{D}\left(\frac{\partial Q}{\partial \boldsymbol{\sigma}}\right)\left(\frac{\partial F}{\partial \boldsymbol{\sigma}}\right)^T \mathbf{D}\left[A + \left(\frac{\partial F}{\partial \boldsymbol{\sigma}}\right)^T \mathbf{D}\left(\frac{\partial Q}{\partial \boldsymbol{\sigma}}\right)\right]^{-1}\right\} d\boldsymbol{\varepsilon} = \mathbf{D}_{ep} d\boldsymbol{\varepsilon}, \tag{25}$$

where $\mathbf{D}_{ep}$ is the elastoplastic matrix. This matrix is symmetric only when associated plasticity holds ($Q = F$). $\mathbf{D}_{ep}$ is defined even when the plasticity is ideal (or perfect) since, in this case, $A = 0$, because F is independent of κ. The difficulty in obtaining matrix $\mathbf{D}_{ep}$ is in the computation of parameter A, up to now unknown. A thermodynamically consistent way of finding A is to admit that κ relates to the work of hardening defined as the work done during plastic deformation, that is,

$$d\kappa = \sigma_1 d\varepsilon_1^p + \sigma_2 d\varepsilon_2^p + ... = \boldsymbol{\sigma}^T d\boldsymbol{\varepsilon}^p. \tag{26}$$

Substitution of Eq. (19) with F replaced by Q into (26) results in

$$d\kappa = d\lambda \boldsymbol{\sigma}^T \frac{\partial Q}{\partial \boldsymbol{\sigma}}. \tag{27}$$

Finally, introducing Eq. (27) into (22),

$$A = -\frac{\partial F}{\partial \kappa}\frac{d\kappa}{d\lambda} = -\frac{\partial F}{\partial \kappa}\boldsymbol{\sigma}^T \frac{\partial Q}{\partial \boldsymbol{\sigma}}. \tag{28}$$

The yield surface F must be known in order to use the relations obtained. The most commonly employed form for metals is the von Mises surface:

$$F = \left[\frac{1}{2}(\sigma_x - \sigma_y)^2 + \frac{1}{2}(\sigma_x - \sigma_z)^2 + \frac{1}{2}(\sigma_y - \sigma_z)^2 + 3\tau_{xy}^2 + 3\tau_{xz}^2 + 3\tau_{yz}^2\right]^{1/2} - Y = \sigma_{VM} - Y, \tag{29}$$

where $Y(\kappa)$ is the uniaxial yield stress and σ_{VM} von Mises stress or second order invariant. Differentiating Eq. (29),

$$\begin{aligned} &\frac{\partial F}{\partial \sigma_x} = \frac{3s_x}{2\sigma_{VM}} \qquad \frac{\partial F}{\partial \sigma_y} = \frac{3s_y}{2\sigma_{VM}} \qquad \frac{\partial F}{\partial \sigma_z} = \frac{3s_z}{2\sigma_{VM}} \\ &\frac{\partial F}{\partial \tau_{xy}} = \frac{3\tau_{xy}}{\sigma_{VM}} \qquad \frac{\partial F}{\partial \tau_{xz}} = \frac{3\tau_{xz}}{\sigma_{VM}} \qquad \frac{\partial F}{\partial \tau_{yz}} = \frac{3\tau_{yz}}{\sigma_{VM}}, \end{aligned} \tag{30}$$

where s_x, s_y e s_z are the deviatoric stresses, i.e., $s_x = \sigma_x - (\sigma_x + \sigma_y + \sigma_z)/3$, etc. If a curve obtained experimentally in a uniaxial test is available providing σ_{VM} versus plastic deformations ε_u^p and, if κ represents the work of hardening, then

$$d\kappa = Y d\varepsilon_u^p \,, \tag{31}$$

and hence,

$$-\frac{\partial F}{\partial \kappa} = \frac{dY}{d\kappa} = \frac{dY}{d\varepsilon_u^p}\frac{d\varepsilon_u^p}{d\kappa} = \frac{1}{Y}\frac{dY}{d\varepsilon_u^p} = \frac{H}{Y} \,, \tag{32}$$

where H is the inclination of the curve obtained from the uniaxial test. Admitting associated plasticity and, substituting Eq. (32) into (28), it can be shown that $A = H$, where H is also known as plasticity modulus. This last expression establishes the well-known Prandtl-Reuss stress × strain relations. The expressions obtained completely describe the stress × strain relations in the elastoplastic state. The nonlinearity is evident from Eq. (25). An algorithm that can be used to solve the nonlinear plastic problem is (Zienkiewicz et al, 1969):

1. Apply load increment and determine corresponding elastic stress increments $\Delta\boldsymbol{\sigma}_1$' and strain increments $\Delta\boldsymbol{\varepsilon}_1$';
2. Add $\Delta\boldsymbol{\sigma}_1$' to the stresses $\boldsymbol{\sigma}_0$ existing prior to the load increment to obtain $\boldsymbol{\sigma}$'. Check if $F(\boldsymbol{\sigma}') < 0$ (κ related to the initial state $\boldsymbol{\sigma}_0$). If the inequality holds, only elastic deformation occurs and the process stops. On the contrary, continue to step 3;
3. If $F(\boldsymbol{\sigma}') \geq 0$ and also $F(\boldsymbol{\sigma}_0) = 0$ (that is, the element was yielded), find $\Delta\boldsymbol{\sigma}_1$ by Eq. (25): $\Delta\boldsymbol{\sigma}_1 = \mathbf{D}_{ep}\,\Delta\boldsymbol{\varepsilon}_1$', with $\mathbf{D}_{ep}$ obtained at state $\boldsymbol{\sigma}$';
4. Compute residual stresses that must be sustained by body forces: $\Delta\boldsymbol{\sigma}_1'' = \Delta\boldsymbol{\sigma}_1' - \Delta\boldsymbol{\sigma}_1$;
5. Store current stress $\boldsymbol{\sigma} = \boldsymbol{\sigma}' - \Delta\boldsymbol{\sigma}_1''$, strain $\boldsymbol{\varepsilon} = \boldsymbol{\varepsilon}' + \Delta\boldsymbol{\varepsilon}_1'$ and displacement $\mathbf{u} = \mathbf{u}' + \Delta\mathbf{u}_1$;
6. If $F(\boldsymbol{\sigma}') \geq 0$ but $F(\boldsymbol{\sigma}_0) < 0$, find the intermediate value of stress when yielding begins and compute $\Delta\boldsymbol{\sigma}_1 = \mathbf{D}_{ep}\,\Delta\boldsymbol{\varepsilon}_1$' from that point;
7. Compute nodal forces corresponding to $\Delta\boldsymbol{\sigma}_1''$, i.e., for each element evaluate $\mathbf{p}^e = \int \boldsymbol{\Phi}^T \Delta\boldsymbol{\sigma}_1'' d\Omega^e$;
8. Solve the new system of equations with the original elastic properties and the global vector $\mathbf{p}$ to find $\Delta\boldsymbol{\sigma}_2$' and $\Delta\boldsymbol{\varepsilon}_2$';
9. Compute the updated value of κ;
10. Repeat 2 thru 9, etc.

The algorithm ends when the nodal forces $\mathbf{p}^e$ are small. If it does not happen in a number of iterations (20 in this work) then collapse condition has been reached.

3.1. Plastic analysis of a damaged pipe

The same pipe simulated in section 2.1 is used in the simulations of plasticity. The yield stress assumed is 400 MPa whereas perfect plasticity is considered, i.e., $A = 0$ in Eq. (25). The pressure is steadily increased until collapse is reached. Figure 5 shows that collapse is suddenly reached at a pressure of about 58 atm. w_{MAX} is the maximum transverse displacement in absolute value. Comparison against the commercial code MSC.Nastran attests to the accuracy of the finite element code implemented. Small discrepancies are observed in the plastic regime because the plasticity models and algorithms do not match exactly.

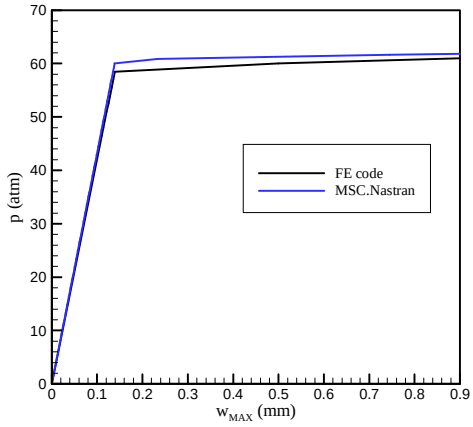

Figure 5. Perfectly plastic response of damaged cylinder

3.2. Plastic analysis of a repaired pipe

The pipe just simulated is now repaired using one layer of AG370-8H /AS4 from Hexel® with 1.0 mm thickness, which corresponds to the depth of the groove damage. The composite repair is made of balanced woven fabrics where the longitudinal and transverse elastic modulus can be assumed equal ($E_1 = E_2$) and, consequently, $\nu_{12} = \nu_{21}$. The volume fraction of fibers and matrix are assumed 50% what leads to the mechanical properties $E_1 = E_2 = 65.18$ GPa, $\nu_{12} = \nu_{21} = 0.05$ and $G_{12} = G_{13} = G_{23} = 4.66$ GPa.

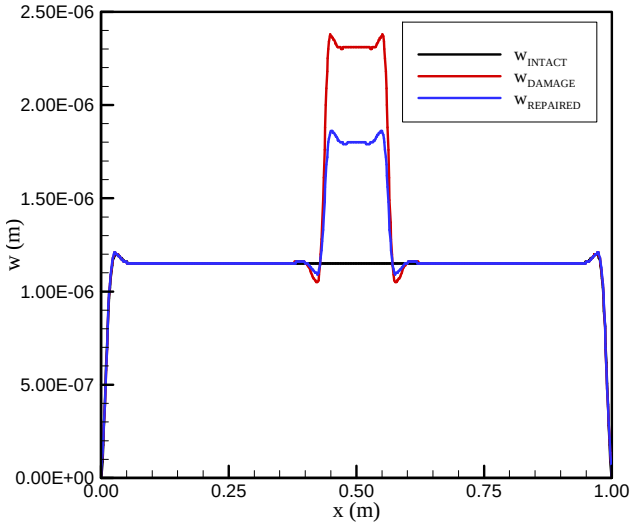

Figure 6. Metallic cylinder with composite repair: edge effects

When an internal pressure of 1 atm is applied the transverse displacements observed are shown in Fig. 6. The beneficial effects of the composite repair can be noticed since the transverse displacement with the damaged zone is now closer to that of the intact cylinder.

A nonlinear plastic analysis of the repaired pipe can be conducted. Plasticity effects are considered to be restricted to the metal, i.e., the composite is layer is assumed to be completely elastic and its strength is assumed infinite. This is not a physically realistic assumption but, since the plastic yield stress adopted is significantly lower than the failure stresses of the composite, this is a reasonable assumption.

Figure 7 shows the result obtained by the simulation. It is obvious that, after a critical pressure is reached, plastic effects take over the metal, significantly reducing its stiffness. Subsequent pressure increments are supported only by the composite repair. The critical pressure is the simulation is about 78 atm.

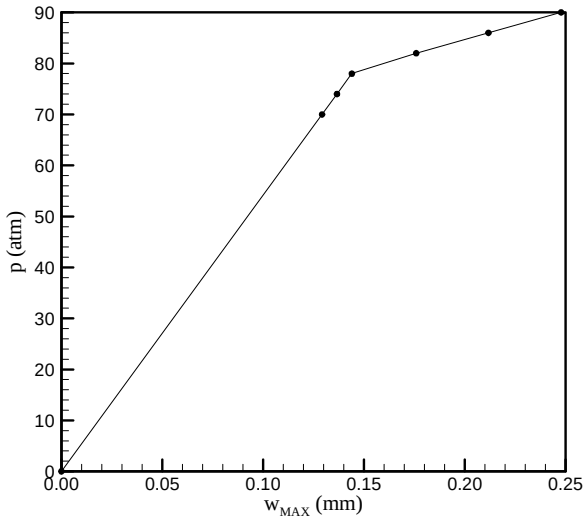

Figure 7. Perfectly plastic response of a repaired cylinder

4. CONCLUSIONS

The critical pressure load observed in the case of a damaged pipe without repair corresponds to the ultimate pressure allowed. Pressure increments beyond that point lead to a sudden collapse as illustrated in Fig. 5. On the other hand, a repaired pipe can sustain pressures substantially beyond the critical pressure where plastic effects become present. An ultimate failure analysis in the case of a repaired pipe would involve the application of composite failure theories and damage progress models.

Figure 6 shows that the composite repair tends to decrease the transverse displacement in the damaged region. The composite material selected as repair has an elastic modulus of 65.18 GPa, which is considerably lower that the 210 GPa of the metal. It is expected that elastic modulus closer to that of the metal would make the jumps observed in Figs. 4 or 6 less pronounced. However, for pressures loadings beyond the critical pressure, a modulus as high as possible would be the primary objective

5. ACKNOWLEDGEMENTS

The authors acknowledge the financial support provided by Eletronorte under grant no. 4500043053.

6. REFERENCES

Almeida, S.M.F., 1982, “Análise e Desenvolvimento da Empenagem de Foguete Utilizando Material Conjugado”, master thesis, Instituto Tecnológico da Aeronáutica, São José dos Campos, Brazil.

Levy Neto, F., 1983, “Estudo de Falha ao Impacto de uma Estrutura de Material Conjugado usado em Aeronaves”, master thesis, Instituto Tecnológico da Aeronáutica, São José dos Campos, Brazil.

Levy Neto, F., Soares, V.B. and Lisboa, W.R., 2000, “Numerical Study of Steel Pipes Repaired with Angle Ply Laminates”, Proceedings of the Congresso Nacional de Engenharia Mecânica, Natal, RN, Brazil.

Levy Neto, F., Maia, G.C. and Ferreira, J.L.A., 2005, “Internally Pressurized Aluminum Pipes Strengthened with a Composite Repair”, Proceedings of the 18th International Congress of Mechanical Engineering, Ouro Preto, MG, Brazil.

Levy Neto, F., Palmério, A.F., 1994, “Structural Behavior of an Aramid Motor Case”, Proceedings of the International Conference on Spacecraft Structures and Mechanical Testing, Paris, France.

Levy Neto, F. and Gonçalves, A., 2001, “Mechanical Evaluation of Panox/phenolic Laminates”, Proceedings of the XVI Congresso Brasileiro de Engenharia Mecânica, Uberlândia, MG, Brazil.

Hughes, T.J.R., 1987, “The Finite Element Method”, Prentice-Hall, New Jersey.

de Faria, A.R., 2000, “Buckling Optimization of Composite Plates and Cylindrical Shells: Uncertain Loading Combinations”, PhD thesis, University of Toronto, Toronto, Canada.

Kachanov, L.M., 2004, “Fundamentals of the Theory of Plasticity”, Dover.

Owen, D.R.J., 1980, “Finite Elements in Plasticity”, Pineridge Press Limited.

Zienkiewicz, O.C., Valliappant, S. and King, I.P., 1969, “Elasto-plastic Solutions of Engineering Problems ‘Initial Stress’, Finite Element Approach”, International Journal for Numerical Methods in Engineering, Vol. 1, pp. 75-100

7. RESPONSIBILITY NOTICE

The authors are the only responsible for the printed material included in this paper.